Developmental Biology 464 (2020) 137–144

Contents lists available at ScienceDirect

Developmental Biology

journal homepage: www.elsevier.com/locate/developmentalbiology

Macrophages fine-tune pupil shape during development

Moe Takahashi [a,b,1], Mika Misaki [a,1], Shinsuke Shibata [c], Takahito Iga [a,d], Tomoko Shindo [c], Ikue Tai-Nagara [a], Ayako Hirata [a], Marina Ogawa [a,e], Takeshi Miyamoto [f], Taneaki Nakagawa [b], Masatsugu Ema [g], Yusuke Ichiyama [h], David T. Shima [i], Katsuto Hozumi [j], Satoshi Nishimura [k], Yoshiaki Kubota [a,*]

[a] Department of Anatomy, Japan
[b] Department of Dentistry and Oral Surgery, Japan
[c] Electron Microscope Laboratory, Japan
[d] Department of Orthopedic Surgery, Keio University School of Medicine, 35 Shinanomachi, Shinjuku-ku, Tokyo, 160-8582, Japan
[e] Department of Ophthalmology, Tokyo Medical University, 6-7-1 Nishi-Shinjuku, Shinjuku-ku, Tokyo, 160-0023, Japan
[f] Department of Orthopedic Surgery, Kumamoto University, 1-1-1 Honjo, Chuo-ku, Kumamoto, 860-8556, Japan
[g] Department of Stem Cells and Human Disease Models, Research Center for Animal Life Science, Japan
[h] Department of Ophthalmology, Shiga University of Medical Science, Seta, Tsukinowa-cho, Otsu, Shiga, 520-2192, Japan
[i] Translational Vision Research, UCL Institute of Ophthalmology, University College London, 11-43 Bath Street, London, EC1V 9EL, UK
[j] Department of Immunology, Tokai University School of Medicine, Isehara, Kanagawa, 259-1193, Japan
[k] Jichi Medical University, 3311-1 Yakushiji, Shimotsuke-shi, Tochigi, 329-0498, Japan

ARTICLE INFO

Keywords:
Macrophage
Pupillary membrane
Retina
Angiogenesis
VEGF
Dll4

ABSTRACT

Tissue macrophages, which are ubiquitously present innate immune cells, play versatile roles in development and organogenesis. During development, macrophages prune transient or unnecessary synapses in neuronal development, and prune blood vessels in vascular development, facilitating appropriate tissue remodeling. In the present study, we identified that macrophages contributed to the development of pupillary morphology. *Csf1*$^{op/op}$ mutant mice, in which ocular macrophages are nearly absent, exhibited abnormal pupillary edges, with abnormal protrusions of excess iris tissue into the pupillary space. Macrophages located near the pupillary edge engulfed pigmented debris, which likely consisted of unnecessary iris protrusions that emerge during smoothening of the pupillary edge. Indeed, pupillary edge macrophages phenotypically possessed some features of M2 macrophages, consistent with robust tissue engulfment and remodeling activities. Interestingly, protruding irises in *Csf1*$^{op/op}$ mice were only detected in gaps between regressing blood vessels. Taken together, our findings uncovered a new role for ocular macrophages, demonstrating that this cell population is important for iris pruning during development.

1. Introduction

Tissue macrophages are mononuclear phagocytes with versatile roles in development, tissue homeostasis, and immunity. Macrophages predominately originate from yolk-sac-derived erythro-myeloid progenitors distinct from hematopoietic stem cells (Gomez Perdiguero et al., 2015), and acquire tissue specificity after entry into the embryo (Mass et al., 2016). Functionally, during embryonic and postnatal development, macrophages regulate remodeling of various organs by removing transient or unnecessary tissues, in particular by pruning synapses (Paolicelli et al., 2011) and blood vessels (Lang and Bishop, 1993; Ishida et al., 2003) during neuronal and vascular development. Macrophage polarization influences their activity in both tissue remodeling and inflammatory responses (Sica and Mantovani, 2012).

During embryogenesis and early postnatal ages in mice, the pupil is closed by a thin vascular membrane called pupillary membrane (PM), which divides the space in which the iris is suspended into two distinct chambers (Ito and Yoshioka, 1999). PM vessels, together with hyaloid vessels (HVs), form the temporary circulatory system in fetal eyes, and gradually regress after birth in mice and by late gestation in humans

* Corresponding author. Keio University School of Medicine, 35 Shinanomachi, Shinjuku-ku, Tokyo 160-8582, Japan.
E-mail address: ykubo33@a3.keio.jp (Y. Kubota).
[1] These authors contributed equally to this paper.

https://doi.org/10.1016/j.ydbio.2020.06.004
Received 13 February 2020; Received in revised form 8 June 2020; Accepted 9 June 2020
Available online 18 June 2020

(Lang and Bishop, 1993; Silbert and Gurwood, 2000; Ito and Yoshioka, 1999). This programmed regression of fetal-type vessels is controlled by macrophages (Lang and Bishop, 1993) and neurons (Yoshikawa et al., 2016). However, the role of macrophages in the remodeling of other ocular components has not been elucidated. In the present study, we used *Csf1*$^{op/op}$ mutant mice, which have a spontaneous null mutant for the *Csf1* gene (Marks and Lane, 1976; Yoshida et al., 1990; Cecchini et al., 1994), resulting in near-complete ocular macrophage depletion. With this model, we identified a novel developmental role for ocular macrophages, which fine-tune the shape of the pupils through engulfment of unnecessary iris tissue.

2. Results

2.1. Visualization and characterization of PM vessels

We previously reported the mechanism for programmed regression of HVs using a whole-mount immunostaining technique (Yoshikawa et al., 2016). In the present study, we first established a procedure to visualize whole-mount structures of PM vessels, other fetal-type vessels in eye balls. Modifying the previous protocol (Poché et al., 2015), we isolated the PM en bloc with the iris as a template and stained the resultant whole-mount immunohistochemically (Fig. 1A). This technique allowed us to examine the whole structure of PM vessels, which were surrounded by macrophages and exhibited active proliferation of endothelial cells on postnatal (P) day 3 (Fig. 1B, C, E, G), but not on P8 (Fig. 1D, F). These data indicated that prior to P6, PM vessels were still growing rather than regressing. Retinal vessels are also actively proliferating at this stage, which is robustly regulated by vascular endothelial growth factor (VEGF) and Notch signaling (Benedito et al., 2012; Zarkada et al., 2015). Therefore, we tested the effects of VEGF receptor 2 (VEGFR2) deletion, or ablation of Dll4, a well-known endothelial Notch ligand (Hellström et al., 2007) (Fig. 1H). When we deleted *Vegfr2* in endothelial cells (ECs) starting at P2 using *Cdh5-BAC-Cre*^{ERT2} mice (*Cdh5–BAC–Cre*$^{ERT2+}$*Vegfr2*$^{flox/flox}$, hereafter referred to as *Vegfr2*$^{i\Delta EC}$), the *Vegfr2*$^{i\Delta EC}$ pups exhibited early regression of PM vessels at P6 (Fig. 1I-L O). Conversely, mice with EC-specific *Dll4* deletion using the same approach (*Cdh5–BAC–Cre*$^{ERT2+}$*Dll4*$^{flox/flox}$, hereafter referred to as *Dll4*$^{i\Delta EC}$) exhibited increased PM vessel density at P6 (Fig. 1M-O). These data suggested that prior to P6, PM vessels were highly plastic, and were vulnerable to disruption of VEGF and Notch signaling, similar to retinal vessels. However, neuronal deletion of *Vegfr2* did not affect PM vessel density (Fig. 1P–S) unlike in HVs (Yoshikawa et al., 2016), suggesting that neuron-derived VEGF may not be involved in PM vessel regression because it cannot reach the anterior chamber of the eye. The regression of PM vessels and HVs is likely to be regulated through distinct mechanisms.

2.2. Macrophage depletion resulted in irregular pupillary edges

A prior report demonstrated that macrophage depletion leads to the persistence of the PM and its vasculature for up to 2 weeks after birth (Lang and Bishop, 1993). However, the status of PM vessels during early neonatal stages, especially the first week after birth, and the regulatory role of macrophages in this context remain unknown. A prior report demonstrated that macrophages contribute to the bridging of tip cell

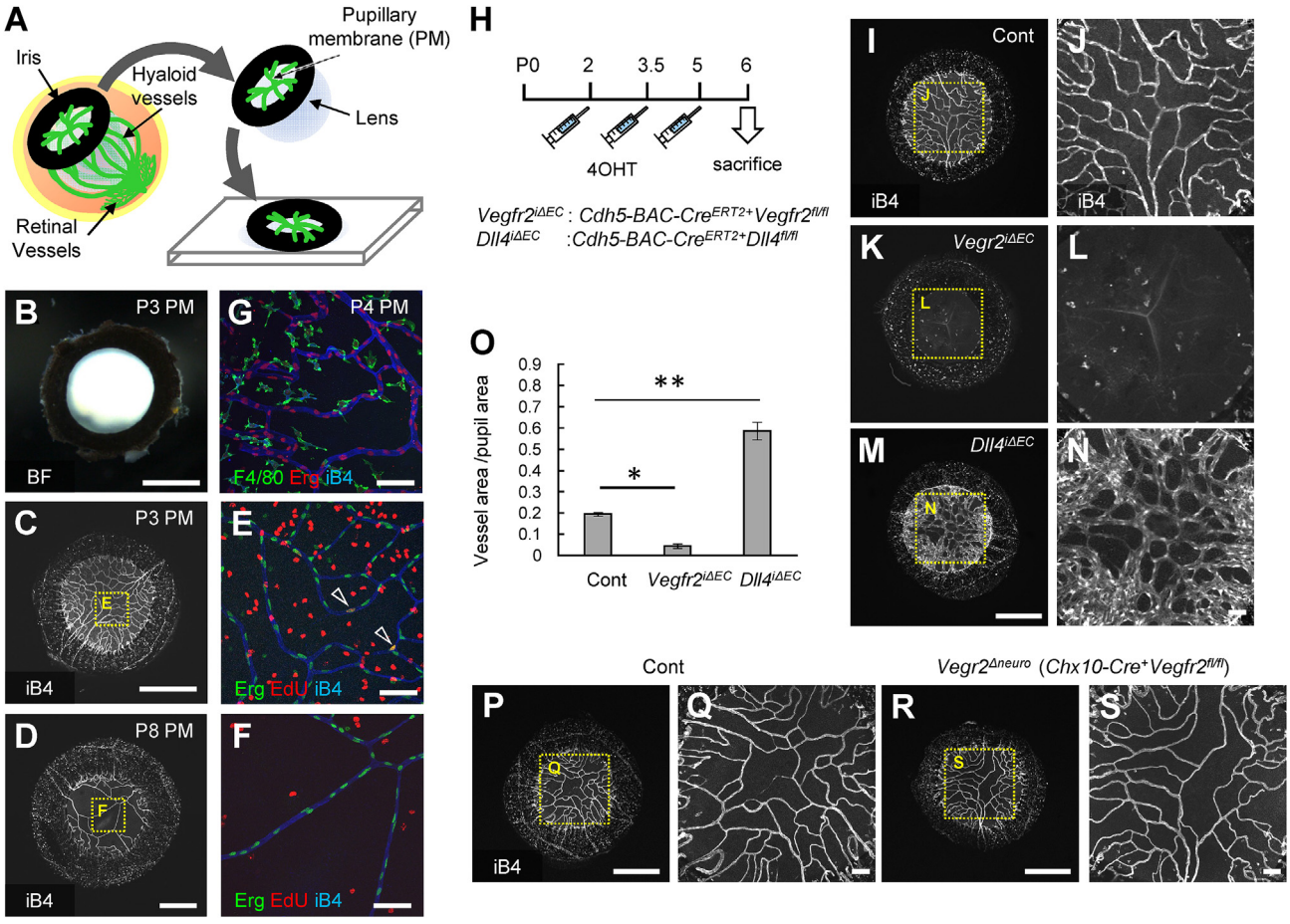

Fig. 1. Visualization and characterization of pupillary membrane vessels. (**A**) Schematic diagram of the technique used to visualize the pupillary membrane (PM) and associated blood vessels. (**B-G**) Bright-field view and whole-mount specimens of PMs. Endothelial cells in PM vessels were actively proliferating (arrowheads) at P3. (**H**) Protocol for 4-hydroxytamoxifen (4OHT) injection in neonates. P, postnatal. (**I–S**) Whole-mount specimens of PMs at P6 stained with Isolectin B4 (iB4) and quantification of vessel area (n ≥ 3). Scale bars: 500 μm (**B-D, I, K, M, P, Q**); 50 μm (**E-G, J, L, N, E, Q S**). $^{**}P < 0.01$; $^{*}P < 0.05$. Data are presented as mean ± SD.

filopodia during blood vessel proliferation, facilitating the formation of new branches in the developing vasculature (Fantin et al., 2010). Therefore, we analyzed the PMs of *Csf1*$^{op/op}$ mutant mice during early development. Bright-field microscopy revealed irregular pupillary edges in P6 *Csf1*$^{op/op}$ mice, marked by the presence of protrusions at the pupillary edge (Fig. 2A–C). Furthermore, we followed the time course of this irregularity and measured the area protruding over pupillary edges. While no significant protrusion was detected by P2 in *Csf1*$^{op/op}$ mice, significant protrusion throughout the pupillary edges was present after P4, in contrast to the smoothened regular edge of pupils in age-matched wild-type mice (Fig. 2D-L). This defect was normalized in *Csf1*$^{op/op}$ mice by weaning age (Fig. 2L), suggesting a potential compensatory mechanism in the absence of ocular macrophages. To evaluate the involvement of PM vessel regression in this phenotype, we examined PM vessels with immunostaining (Fig. 2M-T). Although PM vessels persisted in P24 in *Csf1*$^{op/op}$ mice, in agreement with a previous report (Lang and Bishop, 1993), we identified that neither vessel length nor vessel density significantly differed between wild-type and *Csf1*$^{op/op}$ mice prior to P8 (Fig. 2M-X). These data suggest that the abnormal shape of pupils in P6 *Csf1*$^{op/op}$ mice was independent of PM vessel regression, as the failure of PM vessels to regress in *Csf1*$^{op/op}$ mice occurred 2 weeks after birth.

2.3. Pupillary edge macrophages engulfed pigmented debris

Subsequently, we examined the number and localization of macrophages in neonatal PMs. In wild-type mice, a large number of macrophages was present in the PM, iris, and their marginal zones (Fig. 3A, C). Interestingly, macrophages were more abundant in the periphery than in the center of PMs (Fig. 3A), suggesting a functional role in the peripheral area. As expected, *Csf1*$^{op/op}$ mice were nearly devoid of macrophages, including in the areas around the protrusions, although residual macrophages were preferentially present around the sphincter pupillae muscles (Fig. 3B, D, E). Macrophages in normal skin are capable of ingesting melanin and are termed "melanophages" (Haniffa et al., 2009, 2012). Therefore, we postulated that macrophages present on the pupillary edges could also engulf pigmented debris. DAB (diaminobenzidine)/Giemsa counterstaining of the PM revealed that a large population of Iba1^{+} macrophages in wild-type mice contained cytoplasmic melanin vesicles, suggesting active phagocytosis of pigmented tissue (Fig. 3F and G). Contrastingly, *Csf1*$^{op/op}$ mice lacked pigmented vesicles except for ones in few leftover macrophages (Fig. 3H and I). The analysis of scanning (SEM) and transmission electron microscopy (TEM) confirmed that pupillary macrophages contained phagosomal pigmented debris (Fig. 3J-L). Similarly, transmission detector (TD) analysis indicated that macrophages near the pupillary edges contained pigmented granules (Fig. 3M). The protruded iris tissue present in *Csf1*$^{op/op}$ mice lacked nuclei and was located inside the sphincter pupillae muscles stained with alpha smooth muscle actin (ASMA) (Fig. 3N, O), suggesting that the excess tissue was the protrusion of cellular debris but not invagination. TUNEL-positive pigmented cells were detected around the sphincter pupillae muscles in both wild-type and *Csf1*$^{op/op}$ mice (Fig. 3P–S), suggesting that apoptosis generated debris.

2.4. PM macrophages were M2-like

Macrophages are broadly classified into two activation states: M1 (classically) and M2 (alternatively) activated phenotypes, (Biswas and Mantovani, 2010; Murray et al., 2014). This simplistic *in vitro* based M1/M2 dichotomy provides a conceptual framework for classification of *in vivo* macrophage; M1 macrophages are pro-inflammatory and are important in host defense against pathogens through secretion of pro-inflammatory cytokines such as IL-6 and IFN-γ. By contrast, M2 macrophages reduce inflammatory responses, are highly phagocytic, and

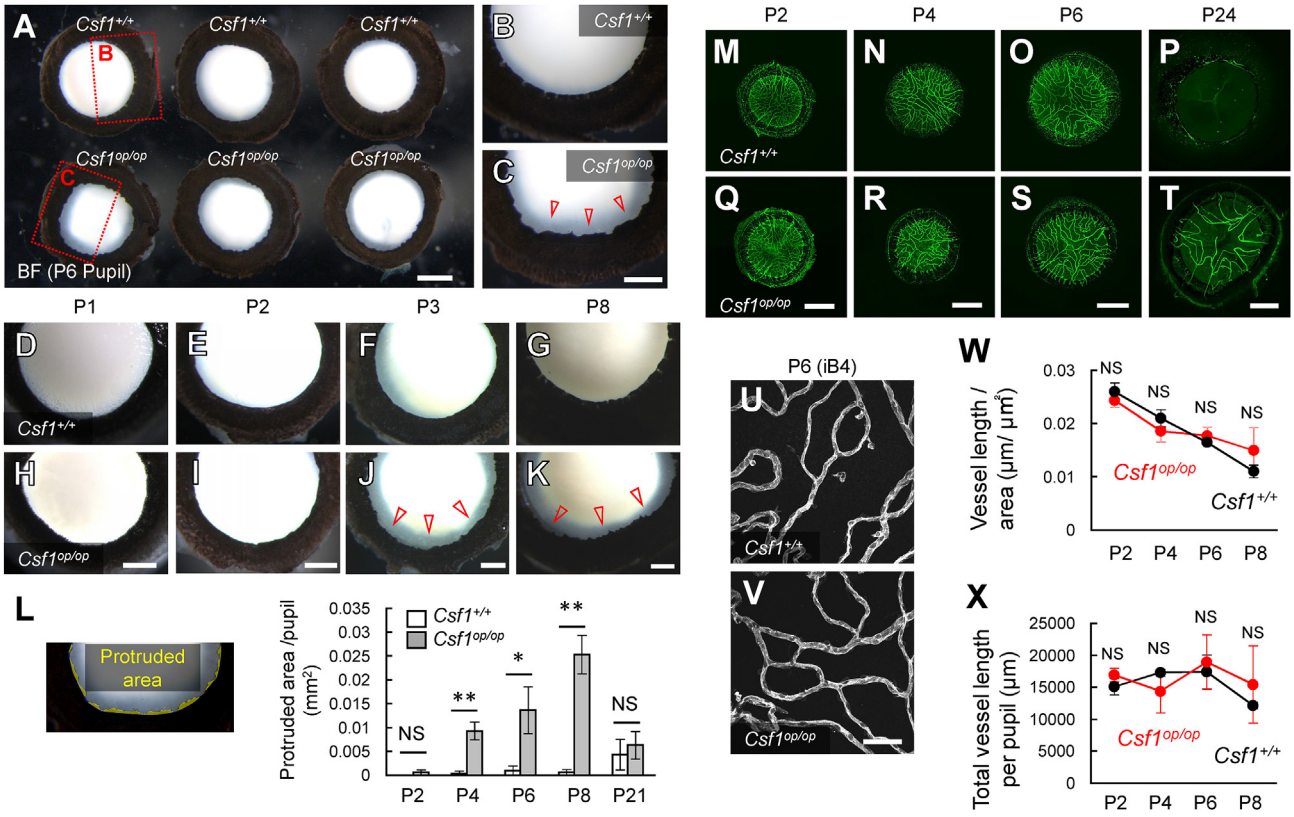

Fig. 2. Absence of macrophages resulted in irregular pupillary edges. (**A-K**) Bright-field views of pupils at P1, P2, P3, P6, and P8. *Csf1*$^{op/op}$ mutant mice exhibited irregular pupillary edges (arrowheads). (**L**) Quantification of the protruding iris, indicated in yellow (n ≥ 3). (**M-X**) Immunohistochemistry of whole-mount PMs at P2, 4, 6, and 24, and quantification of vessel length (n ≥ 3). Scale bars: 500 μm (**A, M-T**); 200 μm (**B–K**); 50 μm (**U, V**). $^{**}P < 0.01$; $^{*}P < 0.05$; NS, not significant. Data are presented as mean ± SD.

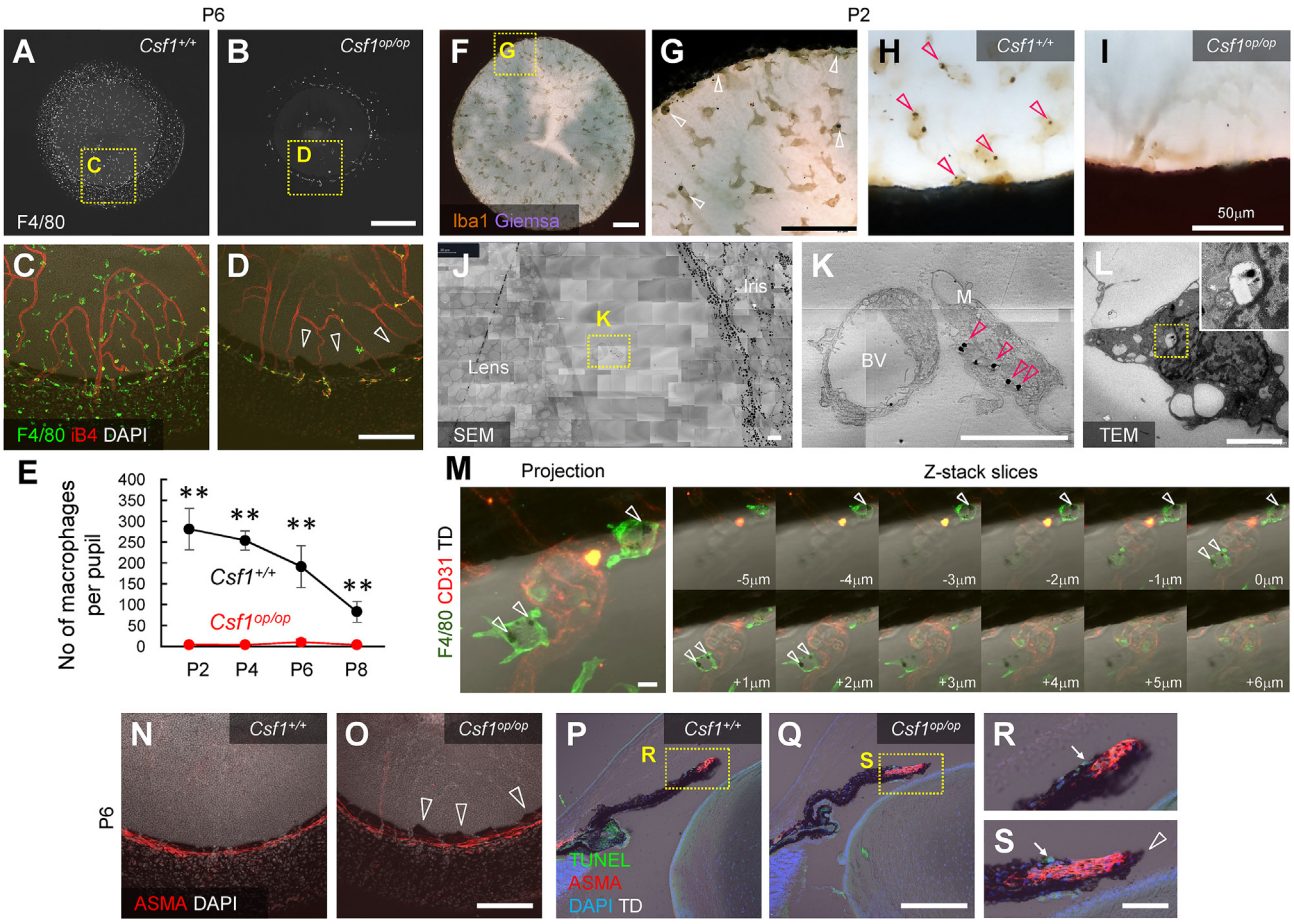

Fig. 3. Macrophages engulfed pigmented debris in the pupillary edges. (**A-D**) Immunohistochemistry of whole-mount PMs at P6. *Csf1*$^{op/op}$ mice lacked macrophages around the irregularly shaped pupillary edges (arrowheads). **(E)** Quantification of macrophages per pupil (n ≥ 3). (**F–I**) Immunohistochemistry of whole-mount PMs at P2. Macrophages around the pupillary edge contained cytoplasmic pigmented granules in wild-type mice (arrowheads). (**J-L**) Scanning (**J**, **K**) or transmission (**L**) electron microscopic analysis of pupillary macrophages containing pigmented granules (arrowheads). (**M**) Immunohistochemistry of whole-mount PM samples at P2. Macrophages contained pigmented granules in the cytoplasm (arrowheads). Both a projection image and z-stack slices at 1 μm intervals are shown. (**N, O**) Immunohistochemistry merged with transmission detector (TD) images in whole-mount PMs at P6. The protruding iris tissue observed in *Csf1*$^{op/op}$ mice was located inside the sphincter pupillae muscles and lacked nuclei (arrowheads). (**P–S**) TUNEL staining combined with immunohistochemistry in eyeball sections at P6. Apoptotic cells were located on the iris (arrows) but not in protruding iris tissue in *Csf1*$^{op/op}$ mutant mice (arrowhead). Scale bars: 500 μm (**A, B**); 200 μm (**C, D, N-Q**); 50 μm (**F–I, R, S**); 5 μm (**J–M**). Data are presented as mean ± SD.

promote tissue remodeling (Biswas and Mantovani, 2010; Sica and Mantovani, 2012; Okuno et al., 2011). Several M2-specific markers have been identified, such as MRC-1, ARG-1, IGF-1, and CSFR1 (Sica and Mantovani, 2012; Spadaro et al., 2017; Ohashi et al., 2017). Considering the morphologies of the pupillary macrophages in the postnatal pupil and the immune privilege in the ocular anterior chamber, we postulated that this cell population was likely to exhibit an M2 phenotype. To assess the phenotype of pupillary macrophages, the relative expression of M1/M2 markers in pupillary macrophages, bone marrow macrophages, and retinal (resting) microglia were quantified at P4. As expected, pupillary macrophages expressed lower M1 and higher M2 markers than bone marrow macrophages, while M2 markers were lowest in microglia (Fig. 4A). Unexpectedly we did not detect Arg1 expression in macrophages suggesting they possess some features of M2 macrophages but not others. Immunohistochemical analysis also revealed that pupillary macrophages were positive for Mrc1, and that Mrc1+ macrophages were highly abundant around the pupillary edge (Fig. 4B–G).

Excess iris tissue protruded between blood vessels in the absence of macrophages.

For pupillary macrophages to smooth pupillary edges, the engulfment of iris tissue must be specific to protruding debris. Therefore, we determined which parts of the pupils protruded (Fig. 5A and B). High magnification microscopy of the pupillary edges revealed that aberrant iris tissue protruded between blood vessels crossing the pupils in *Csf1*$^{op/op}$ mutant mice. In addition, these peri-pupillary vessels looped around the pupillary edges from the upper to lower surfaces of the pupils (hereafter referred to as looping vessels), and appeared to drag in iris tissue (Fig. 5C–E). In the absence of macrophages, excess iris tissue protruded between looping vessels, where this debris would otherwise have been engulfed by pupillary macrophages. To assess the blood flow known to be important for regression of PM vessels (Morizane et al., 2006; Meeson et al., 1996), we utilized *in vivo* imaging of *Vegfr2-BAC-Egfp* mice (Ishitobi et al., 2010). At P3, blood flow was abundant in looping vessels but sparse in central vessels, suggesting that programmed regression of PM vessels was initiated in central vessels (Fig. 5F; Supplementary Movie 1). Labeling erythrocytes with Ter119 antibody revealed abundant erythrocytes in looping vessels, consistent with high blood flow in this region (Fig. 5G). These findings suggested that the looping vessels were stable and physically stiff, we suspected the drag-in force of these vessels on the pupillary edge. To test this hypothesis, we examined the pupil shape of *Vegfr2*$^{i\Delta EC}$ and *Dll4*$^{i\Delta EC}$ mice. Although no apparent protrusions were observed in pupils of *Vegfr2*$^{i\Delta EC}$ and *Dll4*$^{i\Delta EC}$ mice, the overall width of pupillary edges looks wider in *Vegfr2*$^{i\Delta EC}$ than in wild-type mice (new Fig. 5H and I), likely due to the absence of drag-in

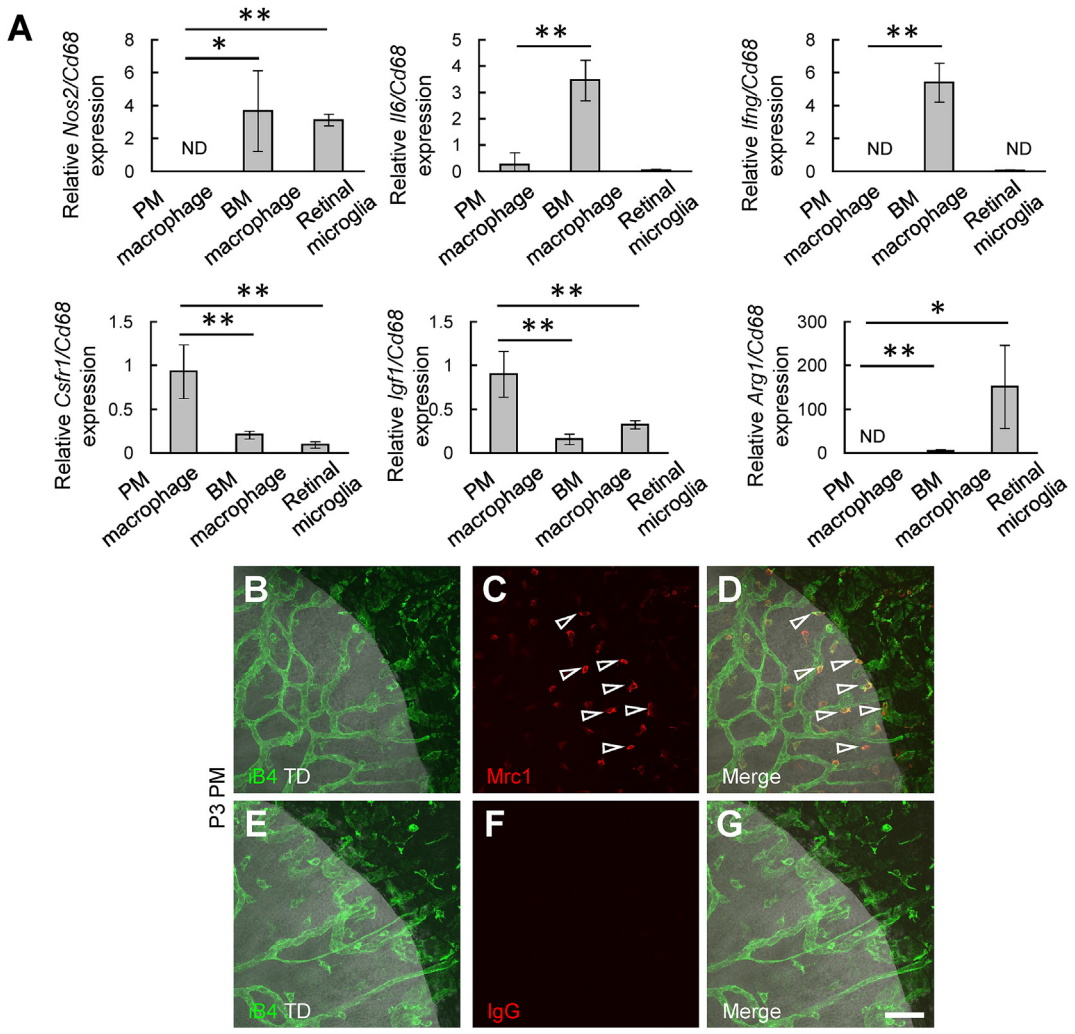

Fig. 4. Macrophages in the pupillary membrane exhibited an M2-like phenotype. (**A**) Quantitative PCR analysis of pupillary macrophages, bone marrow macrophages, and retinal microglia at P4 (n = 3/group). All values are normalized by the expression of *Cd68*. (**B-G**) Immunohistochemistry merged with transmission detector (TD) images in whole-mount PMs at P3. $Mrc1^{+}$ macrophages were present around the pupillary edge (arrowheads). Scale bar, 50 μm $^{**}P < 0.01$; $^{*}P < 0.05$. Data are presented as mean ± SD.

forces of looping vessels. We did not detect any abnormalities in the pupils of $Dll4^{i\Delta EC}$ mice (new Fig. 5J). All of these data suggested that both looping vessels and macrophages are required for regulating the shape of the developing pupil.

3. Discussion

In the present study, we identified a novel role for macrophages in ocular development in regulating the shape of the developing pupil. Macrophages smooth the pupillary edges by engulfing enucleated pigmented iris debris between looping blood vessels. In the absence of macrophages, the debris protruded between the looping vessels and into the pupillary space, resulting in an irregular pupillary edge (Fig. 5K).

Numerous prior studies have reported that macrophages control the formation and regression of ocular blood vessels (Lang and Bishop, 1993; Kubota et al., 2009; Fantin et al., 2010). However, the orchestration of macrophages and blood vessels in remodeling other tissue types has not been extensively investigated. Our present study indicated the cooperation of macrophages and blood vessels in regulating formation of the pupillary edge. However, pupils in $Csf1^{op/op}$ mice exhibited normal morphology by P21, suggesting a compensatory mechanism, or that the remaining macrophages in $Csf1^{op/op}$ mice were sufficient to ultimately dispose of the debris. Alternatively, the number of pupillary macrophages decreased after P6 in wild-type mice (Fig. 3E), so the functional significance of pupillary macrophages could diminish after this time point.

The eye is often analogized to a sophisticated camera. The iris, which surrounds the pupil, functions as a shutter. A recent study indicated a striking correlation between terrestrial species' ecological niches and pupillary shapes, underscoring the importance of the pupillary shape in survival (Banks et al., 2015). In this study, we uncovered a new regulatory mechanism for the shaping of murine pupils, in which macrophages regulate pupil shape independently of blood vessel regression. M2-like macrophages at the pupillary edge phagocytosed iris debris during the process of pupillary enlargement, which was initiated by looping vessels dragging in excess tissue at the pupillary edge.

The irregularly shaped pupils of $Csf1^{op/op}$ mutant mice were similar to pupillary irregularities observed in posterior synechia. This syndrome is one of the major complications of intraocular surgery, and causes photophobia, pupillary block, and poor eyesight. Because inflammation in the anterior chamber provokes synechia between the iris and peripheral structures, short-acting mydriatics and topical steroid injections can mitigate the severity of synechia (Lee et al., 2009; Shinoda et al., 2001). In the present study, we demonstrated that M2-like macrophages contributed to developmental remodeling of the pupillary shape. Therefore, modulation of macrophage polarization could be an effective treatment strategy for

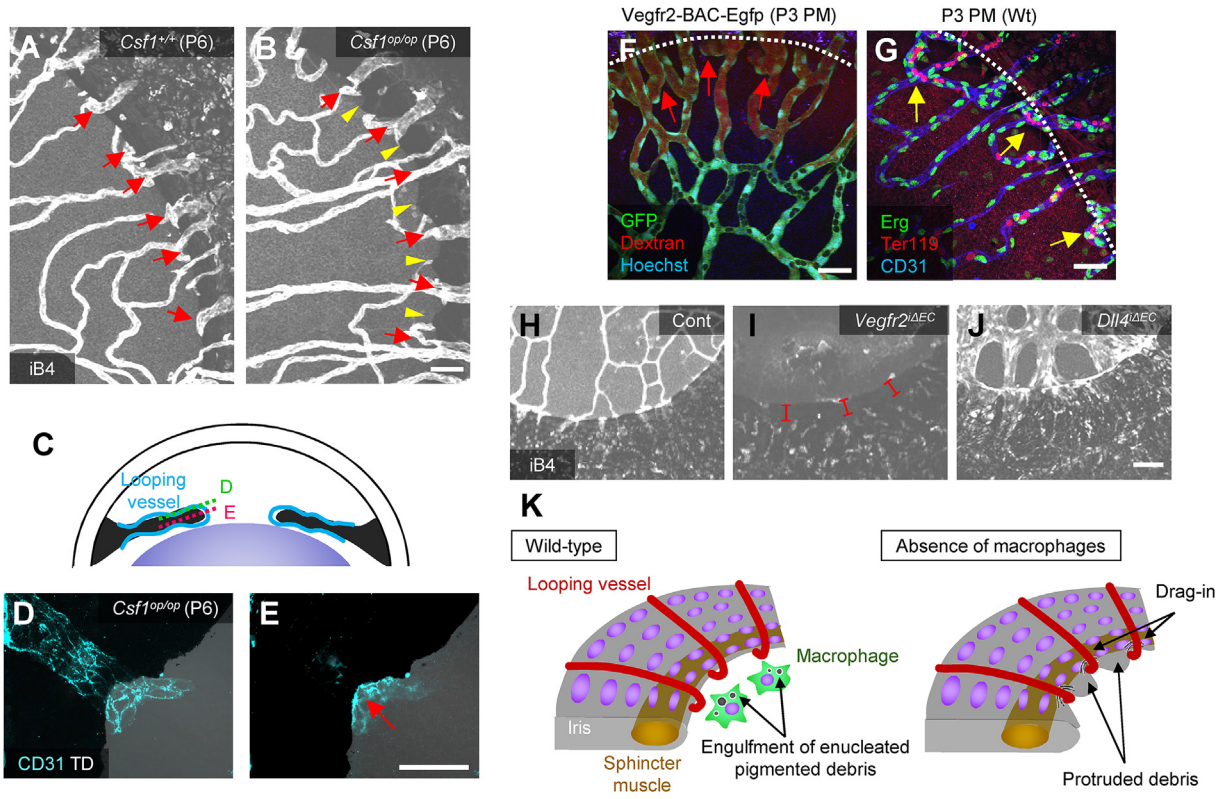

Fig. 5. Pupils protruded between blood vessels in the absence of macrophages. (**A, B**) Immunohistochemistry of whole-mount PMs at P6. Protruded irises (arrowheads) were detected between blood vessels (arrows) in *Csf1*$^{op/op}$ mutant mice. (**C-E**) Immunohistochemistry merged with TD images in whole-mount pupils at P6. Each image depicts a slice, as indicated in the schema in **C**. Blood vessels appeared to loop over the pupillary edges (arrow). (**F**) A snapshot of *in vivo* imaging of the PM of P3 *Vegfr2-BAC-Egfp* mice. Arrows indicate abundant blood flow in looping vessels around the pupillary edges (white line). (**G**) Immunohistochemical analysis of PMs at P3. Abundant erythrocytes were detected in looping vessels (arrows) around the pupillary edges (white line). (**H-J**) Immunohistochemistry of whole-mount PMs at P6. The width of pupillary edges is wider in *Vegfr2*$^{i\Delta EC}$ (red lines) than in control mice. (**K**) Proposed model for macrophage regulation of the pupil shape. Scale bars, 50 μm.

posterior synechia.

Together, the present results revealed a novel developmental function of macrophages, in which this cell population regulates pupillary shape. This finding could further the understanding of ocular autoimmunity.

3.1. Summary statement

Tissue macrophages are mononuclear phagocytes with diverse functions in development, tissue homeostasis, and immunity. The present study demonstrated that during postnatal murine development, macrophages engulfed unnecessary pupillary tissues and contributed to fine tuning of the pupillary shape.

4. Materials and methods

4.1. Mice and analysis

All procedures involving animals were approved by the Institutional Animal Care and Use Committee of Keio University or the Ethical Committee of Jichi Medical University, and were performed in accordance with the guidelines of those universities. C57BL/6 J mice (Japan SLC, Inc., Shizuoka, Japan), *Chx10-Cre* mice (Stock No: 05564; RIKEN BRC) (Muranishi et al., 2011), and *Csf1*$^{op/op}$ mutant mice (Stock No: 000231; Jackson Laboratory) were used. *Cdh5-BAC-Cre*^{ERT2} (Okabe et al., 2014), *Vegfr2-flox* (Okabe et al., 2014), *Dll4-flox* (Hozumi et al., 2008), and *Vegfr2-BAC-Egfp* (Ishitobi et al., 2010) mice were developed previously. Mice of both sexes were included in analysis without sex determination. All mice were crossed with C57BL/6 J mice more than eight times and maintained in this background, except for *Csf1*$^{op/op}$ mutant mice, which were maintained in the B6C3FeF1/J a/a background.

4.2. Preparation of whole-mount PM

Enucleated eyes were fixed for 20 min in 4% paraformaldehyde in phosphate-buffered saline (PBS) and subsequently dissected. A small hole was made in the edge of the cornea using a 27-gauge needle, and a circular incision was made using fine scissors. The cornea and lens were isolated en bloc with the iris, which acted as a frame, followed by dissection of the posterior side of lens. The whole-mount tissues were post-fixed overnight and subsequently stained as described below.

4.3. Preparation of tissue sections

Enucleated eyes were fixed for 20 min in 4% paraformaldehyde (PFA) in PBS, and the hemispheres were then cut. After overnight post-fixation, the samples were snap frozen in optimal cutting temperature compound (Sakura Finetechnical, Tokyo, Japan). All specimens were sectioned to a thickness of 14 μm.

4.4. Immunostaining

Immunohistochemistry (IHC) of whole-mount samples or tissue sections was performed as previously described (Kubota et al., 2009). The primary monoclonal antibodies used were hamster anti-CD31 (2H8; 1:1000; Chemicon, Temecula, CA), anti-Ter119 (MAB1125; 1:1000; R&D Systems, Minneapolis, MN), α-smooth muscle actin-Cy3-conjugated (C6198; 1:500;

Sigma-Aldrich, Saint Louis, MO), and F4/80 (Serotec; MCA497R). The primary polyclonal antibodies used were anti-GFP (Alexa488-conjugated; 1:1000; Molecular Probes, Eugene, OR), Erg (ab92513; 1:2000; Abcam, Cambridge, UK), Iba1 (1:1000; WAKO, Osaka, Japan), and Mrc1 (AF2535; 1:100; R&D Systems, Minneapolis, MN).

Secondary antibodies included Alexa 488 fluorescence-conjugated IgGs (Molecular Probes), DyLight549/DyeLight649-conjugated IgGs, or HRP-conjugated IgGs (Jackson ImmunoResearch, West Grove, PA). For nuclear staining, specimens were treated with 4′,6-diamidino-2-phenylindole (DAPI) prior to mounting. In some experiments, blood vessels and monocyte lineage cells were simultaneously visualized using biotinylated isolectin B4 (B-1205; Vector Laboratories), followed by fluorescent streptavidin conjugates (Molecular Probes). For TUNEL assays, tissue sections were stained using the ApopTag Fluorescein In situ Apoptosis Detection - Kit (Chemicon), according to the manufacturer's instructions. To analyze cell proliferation *in vivo*, a 5-ethynyl-2′-deoxyuridine (EdU) incorporation assay using Click-iT EdU Imaging Kits (Invitrogen) was performed according to the manufacturer's instructions. Briefly, 50 μl EdU dissolved in DMSO/PBS (1:4; final concentration, 0.5 mg/ml) was injected intraperitoneally into P8 mice 6 h before sacrifice. For Giemsa staining, Giemsa's Azur Eosin Methylene Blue solution (Merck, Temecula, CA) was used.

4.5. Quantitative PCR analysis

Ocular, retinal, and bone marrow tissues collected for from five P4 mice were incubated for 30 min at 37 °C in DMEM containing 1% collagenase D (from *Clostridium histolyticum*; Sigma-Aldrich), 1 U/ml dispase (Thermo Fisher Scientific, Waltham, MA), and 1 U/ml DNase (Invitrogen, Carlsbad, CA) before cell dissociation by gentle trituration. Cells were isolated using Dynabeads (Veritas, Tokyo, Japan) according to the manufacturer's instructions. To isolate macrophages, dissociated cells were incubated with an anti-F4/80 antibody pre-conjugated to Dynabeads M-450 anti-Rat IgG (DB11035; Veritas). Cells were positively selected, and total RNA was prepared using RNeasy Mini Kit (QIAGEN, Hilden, Germany) according to the manufacturer's instructions. Reverse transcription was performed using Superscript II (Invitrogen). Quantitative PCR assays were performed using an ABI 7500 Fast Real-Time PCR System with TaqMan Fast Universal PCR master mix (Applied Biosystems) and TaqMan Gene Expression Assay Mix with mouse *Csf1r* (Mm00432689_m1), *Ifng* (Mm00801778_m1), *Igf1* (Mm00439560_m1), *Il6* (Mm00446190_m1), *Nos2* (Mm00440502_m1), or *Cd68* (Mm03047343_m1) primers. A mouse *β-Actin* (Mm00607939_s1) assay mix served as an endogenous control. Data were analyzed using 7500 Fast System SDS Software 1.3.1. Each experiment was performed with four replicates from each sample, and the results were averaged.

4.6. In vivo imaging

In vivo analysis for the PM of P3 pups was performed as described previously (Nishimura et al., 2012). In brief, P3 mice were injected with TexasRed Dextran (MW 70 kDa; Thermo Fisher Scientific) intravenously, and time-lapse images of ocular surfaces were then acquired using a resonance-scanning confocal microscope (Nikon A1R System). The collected images were analyzed by observers blinded to sample group using NIS-Elements software (Nikon).

4.7. Electron microscope (EM) analysis

Ocular samples were prepared for EM observation as described previously (Shibata et al., 2015, 2019). Briefly, the tissues were dissected from 2-day-old mice (n = 8), and fixed with 2.5% glutaraldehyde in 0.1 M phosphate buffer (PB; pH 7.4; Muto Pure Chemicals, Tokyo, Japan) for 24 h at 4 °C. After 2 h of post-fixation with 1.0% OsO_4 (TAAB Laboratories Equipment Ltd., England, UK), samples were dehydrated in a series of increasing concentrations of ethanol (70–100%), and then in acetone (Sigma-Aldrich), n-butyl glycidyl ether (QY1; Oken-shoji Co. Ltd., Tokyo, Japan), and graded concentrations of Epon by QY-1. Samples were then incubated in 100% Epon (100 g Epon is composed of 27.0 g MNA, 51.3 g EPOK-812, 21.9 g DDSA, and 1.1 ml DMP-30, all from Oken-shoji Co. Ltd.) for 72 h at 4 °C to enhance the infiltration of the resin. After 72 h of polymerization in 100% Epon at 60 °C, semithin-sections (1 μm thickness) were prepared with a glass knife and stained with toluidine blue. Ultrathin-sections (70 nm thickness) were prepared using an ultramicrotome (Leica UC7; Leica Biosystems, Wetzlar, Germany) with a diamond knife, collected every 10 slices on the cupper grids, and also on the silicon wafer. Ultrathin-sections were stained with uranyl acetate and subsequently lead citrate for 10 min, respectively. The dried up sections on the cupper grids were examined with a TEM (JEM-1400plus; JEOL, Tokyo, Japan), and the sections on the silicon wafer were imaged with a Multibeam Scanning electron microscopy (MultiSEM 505, Carl Zeiss, Oberkochen, Germany).

4.8. Confocal microscopy

Fluorescent images were obtained using a confocal laser scanning microscope (FV1000; Olympus, Tokyo, Japan). Multiple slices horizontally imaged from the same field of view at 0.5 μm intervals were integrated to construct three-dimensional images using an FV10-ASW Viewer (Olympus). For quantifying total vessel length, we measured and summed up the length of all blood vessels existing inside the pupillary circle using the length measuring function of FV10-ASW Viewer (Olympus). To calculate the vessel density based on the total vessel length described above, the area of pupillary circle was measured using Image J Software (NIH, Bethesda, MD, USA).

4.9. Statistics

Results were expressed as mean ± S.D. Comparisons between the averages of two groups were evaluated using an unpaired, two-tailed Student's *t*-test. *P*-values <0.05 were considered statistically significant.

Author contributions statement

Designed experiments: Y.K. Performed experiments: M.T., M.M., S.S., T.S., I.T-N., M.O., A.H., and S.N. Data analysis: M.T., M.M., S.S., T.I., K.O., Y.I., and Y.K. Provided experimental materials: T.M. and M.E. Manuscript editing: T.N. Manuscript composition: M.M. and Y.K.

Funding

This work was supported by Grants-in-Aid for Specially Promoted Research from the Ministry of Education, Culture, Sports, Science, and Technology of Japan (22122002, 25713059, 18H05042, 18K19553, 17K15625, 18K16997, and 19K07389), by AMED-PRIME (JP19gm 6210017h0001, JP20gm6210017h0002), and by research grants from the Takeda Science Foundation, Kao Foundation for Arts and Culture, Mochida Memorial Foundation, Mitsubishi Foundation, Cell Science Research Foundation, SENSHIN Medical Research Foundation, Sumitomo Foundation, Daiichi Sankyo Foundation of Life Science, Naito Foundation, Inamori Foundation, Uehara Memorial Foundation, and Toray Science Foundation.

Declaration of competing interest

The authors declare no conflicts of interest.

Appendix A. Supplementary data

Supplementary data related to this article can be found at https://doi.org/10.1016/j.ydbio.2020.06.004.

References

Banks, M.S., Sprague, W.W., Schmoll, J., Parnell, J.A.Q., Love, G.D., 2015. Why do animal eyes have pupils of different shapes? Sci. Adv. 1 (7), e1500391.

Benedito, R., Rocha, S.F., Woeste, M., Zamykal, M., Radtke, F., Casanovas, O., Duarte, A., Pytowski, B., Adams, R.H., 2012. Notch-dependent VEGFR3 upregulation allows angiogenesis without VEGF-VEGFR2 signalling. Nature 484, 110–114.

Biswas, S.K., Mantovani, A., 2010. Macrophage plasticity and interaction with lymphocyte subsets: cancer as a paradigm. Nat. Immunol. 11, 889–896.

Cecchini, M.G., Dominguez, M.G., Mocci, S., Wetterwald, A., Felix, R., Fleisch, H., O Chisholm, O., Hofstetter, W., Pollard, J.W., Stanley, E.R., 1994. Role of colony stimulating factor-1 in the establishment and regulation of tissue macrophages during postnatal development of the mouse. Development 120, 1357–1372.

Fantin, A., Vieira, J.M., Gestri, G., Denti, L., Schwarz, Q., Prykhozhij, S., Peri, F., Wilson, S.W., Ruhrberg, C., 2010. Tissue macrophages act as cellular chaperones for vascular anastomosis downstream of VEGF-mediated endothelial tip cell induction. Blood 116, 829–840.

Gomez Perdiguero, E., Klapproth, K., Schulz, C., Busch, K., Azzoni, E., Crozet, L., Garner, H., Trouillet, C., de Bruijn, M.F., Geissmann, F., Rodewald, H.R., 2015. Tissue-resident macrophages originate from yolk-sac-derived erythro-myeloid progenitors. Nature 518, 547–551.

Haniffa, M., Ginhoux, F., Wang, X.N., Bigley, V., Abel, M., Dimmick, I., Bullock, S., Grisotto, M., Booth, T., Taub, P., et al., 2009. Differential rates of replacement of human dermal dendritic cells and macrophages during hematopoietic stem cell transplantation. J. Exp. Med. 206, 371–385.

Haniffa, M., Shin, A., Bigley, V., McGovern, N., Teo, P., See, P., Wasan, P.S., Wang, X.N., Malinarich, F., Malleret, B., et al., 2012. Human tissues contain CD141hi cross-presenting dendritic cells with functional homology to mouse CD103+ nonlymphoid dendritic cells. Immunity 37, 60–73.

Hellström, M., Phng, L.K., Hofmann, J.J., Wallgard, E., Coultas, L., Lindblom, P., Alva, J., Nilsson, A.K., Karlsson, L., Gaiano, N., Yoon, K., Rossant, J., Iruela-Arispe, M.L., Kalén, M., Gerhardt, H., Betsholtz, C., 2007. Dll4 signalling through Notch1 regulates formation of tip cells during angiogenesis. Nature 445, 776–780.

Hozumi, K., Mailhos, C., Negishi, N., Hirano, K., Yahata, T., Ando, K., Zuklys, S., Holländer, G.A., Shima, D.T., Habu, S., 2008. Delta-like 4 is indispensable in thymic environment specific for T cell development. J. Exp. Med. 205, 2507–2513.

Ishida, S., Yamashiro, K., Usui, T., Kaji, Y., Ogura, Y., Hida, T., Honda, Y., Oguchi, Y., Adamis, A.P., 2003. Leukocytes mediate retinal vascular remodeling during development and vaso-obliteration in disease. Nat. Med. 9, 781–788.

Ishitobi, H., Matsumoto, K., Azami, T., Itoh, F., Itoh, S., Takahashi, S., Ema, M., 2010. Flk1-GFP BAC Tg mice: an animal model for the study of blood vessel development. Exp. Anim. 59, 615–622.

Ito, M., Yoshioka, M., 1999. Regression of the hyaloid vessels and pupillary membrane of the mouse. Anat. Embryol. 200, 403–411.

Kubota, Y., Takubo, K., Shimizu, T., Ohno, H., Kishi, K., Shibuya, M., Saya, H., Suda, T., 2009. M-CSF inhibition selectively targets pathological angiogenesis and lymphangiogenesis. J. Exp. Med. 206, 1089–1102.

Lang, R.A., Bishop, J.M., 1993. Macrophages are required for cell death and tissue remodeling in the developing mouse eye. Cell 74, 453–462.

Lee, S.B., Lee, D.G., Kwag, J.Y., Kim, J.Y., 2009. The effect of mydriatics on posterior synechia after combined pars plana vitrectomy, phacoemulsification, and intraocular lens implantation. Retina 29 (8), 1150–1154.

Marks Jr., S.C., Lane, P.W., 1976. Osteopetrosis, a new recessive skeletal mutation on chromosome 12 of the mouse. J. Hered. 67, 11–18.

Mass, E., Ballesteros, I., Farlik, M., Halbritter, F., Günther, P., Crozet, L., Jacome-Galarza, C.E., Händler, K., Klughammer, J., Kobayashi, Y., Gomez-Perdiguero, E., Schultze, J.L., Beyer, M., Bock, C., Geissmann, F., 2016. Specification of tissue-resident macrophages during organogenesis. Science 353, aaf4238.

Meeson, A., Palmer, M., Calfon, M., Lang, R., 1996. A relationship between apoptosis and flow during programmed capillary regression is revealed by vital analysis. Development 122, 3929–3938.

Morizane, Y., Mohri, S., Kosaka, J., Toné, S., Kiyooka, T., Miyasaka, T., Shimizu, J., Ogasawara, Y., Shiraga, F., Minatogawa, Y., Sasaki, J., Ohtsuki, H., Kajiya, F., 2006. Iris movement mediates vascular apoptosis during rat pupillary membrane regression. Am. J. Physiol. Regul. Integr. Comp. Physiol. 290, R819–R825.

Muranishi, Y., Terada, K., Inoue, T., Katoh, K., Tsujii, T., Sanuki, R., Kurokawa, D., Aizawa, S., Tamaki, Y., Furukawa, T., 2011. An essential role for RAX homeoprotein and NOTCH-HES signaling in Otx2 expression in embryonic retinal photoreceptor cell fate determination. J. Neurosci. 31, 16792–16807.

Murray, P.J., Allen, J.E., Biswas, S.K., Fisher, E.A., Gilroy, D.W., Goerdt, S., Gordon, S., Hamilton, J.A., Ivashkiv, L.B., Lawrence, T., Locati, M., Mantovani, A., Martinez, F.O., Mege, J.L., Mosser, D.M., Natoli, G., Saeij, J.P., Schultze, J.L., Shirey, K.A., Sica, A., Suttles, J., Udalova, I., van Ginderachter, J.A., Vogel, S.N., Wynn, T.A., 2014. Macrophage activation and polarization: nomenclature and experimental guidelines. Immunity 41, 14–20.

Nishimura, S., Manabe, I., Nagasaki, M., Kakuta, S., Iwakura, Y., Takayama, N., Ooehara, J., Otsu, M., Kamiya, A., Petrich, B.G., Urano, T., Kadono, T., Sato, S., Aiba, A., Yamashita, H., Sugiura, S., Kadowaki, T., Nakauchi, H., Eto, K., Nagai, R., 2012. In vivo imaging visualizes discoid platelet aggregations without endothelium disruption and implicates contribution of inflammatory cytokine and integrin signaling. Blood 119, e45–56.

Ohashi, T., Aoki, M., Tomita, H., Akazawa, T., Sato, K., Kuze, B., Mizuta, K., Hara, A., Nagaoka, H., Inoue, N., Ito, Y., 2017. M2-like macrophage polarization in high lactic acid-producing head and neck cancer. Canc. Sci. 108, 1128–1134.

Okabe, K., Kobayashi, S., Yamada, T., Kurihara, T., Tai-Nagara, I., Miyamoto, T., Mukouyama, Y.S., Sato, T.N., Suda, T., Ema, M., Kubota, Y., 2014. Neurons limit angiogenesis by titrating VEGF in retina. Cell 159, 584–596.

Okuno, Y., Nakamura-Ishizu, A., Kishi, K., Suda, T., Kubota, Y., 2011. Bone marrow-derived cells serve as proangiogenic macrophages but not endothelial cells in wound healing. Blood 117, 5264–5272.

Paolicelli, R.C., Bolasco, G., Pagani, F., Maggi, L., Scianni, M., Panzanelli, P., Giustetto, M., Ferreira, T.A., Guiducci, E., Dumas, L., Ragozzino, D., Gross, C.T., 2011. Synaptic pruning by microglia is necessary for normal brain development. Science 333, 1456–1458.

Poché, R.A., Hsu, C.W., McElwee, M.L., Burns, A.R., Dickinson, M.E., 2015. Macrophages engulf endothelial cell membrane particles preceding pupillary membrane capillary regression. Dev. Biol. 403, 30–42.

Shibata, S., Murota, Y., Nishimoto, Y., Yoshimura, M., Nagai, T., Okano, H., Siomi, M.C., 2015. Immuno-electron microscopy and electron microscopic in situ hybridization for visualizing piRNA biogenesis bodies in Drosophila ovaries. Methods Mol. Biol. 1328, 163–178.

Shibata, S., Iseda, T., Mitsuhashi, T., Oka, A., Shindo, T., Moritoki, N., Nagai, T., Otsubo, S., Inoue, T., Sasaki, E., Akazawa, C., Takahashi, T., Schalek, R., Lichtman, J.W., Okano, H., 2019. Large-area fluorescence and electron microscopic correlative imaging with multibeam scanning electron microscopy. Front. Neural Circ. 13, 00029. eCollection.

Shinoda, K., Ohira, A., Ishida, S., Hoshide, M., Ogawa, L.S., Ozava, Y., 2001. Posterior synechia of the iris after combined pars plana vitrectomy, phacoemulsification and intraocular lens implantation. Jpn. J. Ophthalmol. 45, 276–280.

Sica, A., Mantovani, A., 2012. Macrophage plasticity and polarization: in vivo veritas. J. Clin. Invest. 122, 787–795.

Silbert, M., Gurwood, A.S., 2000. Persistent hyperplastic primary vitreous. Clin. Eye Vis. Care 12, 131–137.

Spadaro, O., Camell, C.D., Bosurgi, L., Nguyen, K.Y., Youm, Y.H., Rothlin, C.V., Dixit, V.D., 2017. IGF1 shapes macrophage activation in response to immunometabolic challenge. Cell Rep. 19, 225–234.

Yoshida, H., Hayashi, S., Kunisada, T., Ogawa, M., Nishikawa, S., Okamura, H., Sudo, T., Shultz, L.D., Nishikawa, S., 1990. The murine mutation osteopetrosis is in the coding region of the macrophage colony stimulating factor gene. Nature 345, 442–444.

Yoshikawa, Y., Yamada, T., Tai-Nagara, I., Okabe, K., Kitagawa, Y., Ema, M., Kubota, Y., 2016. Developmental regression of hyaloid vasculature is triggered by neurons. J. Exp. Med. 213, 1175–1183.

Zarkada, G., Heinolainen, K., Makinen, T., Kubota, Y., Alitalo, K., 2015. VEGFR3 does not sustain retinal angiogenesis without VEGFR2. Proc. Natl. Acad. Sci. U.S.A. 112, 761–766.